Supplemental Information

Transcriptome analysis uncovers a growth-promoting activity of orosomucoid-1 on hepatocytes

Xian-Yang Qin, Mitsuko Hara, Erik Arner, Yoshikuni Kawaguchi, Ikuyo Inoue, Hideki Tatsukawa, Yutaka Furutani, Keisuke Nagatsuma, Tomokazu Matsuura, Feifei Wei, Jun Kikuchi, Hideko Sone, Carsten Daub, Hideya Kawaji, Timo Lassmann, Masayoshi Itoh, Harukazu Suzuki, Piero Carninci, Yoshihide Hayashizaki, the FANTOM consortium, Norihiro Kokudo, Alistair R. R. Forrest, and Soichi Kojima

Supplemental Figure 1

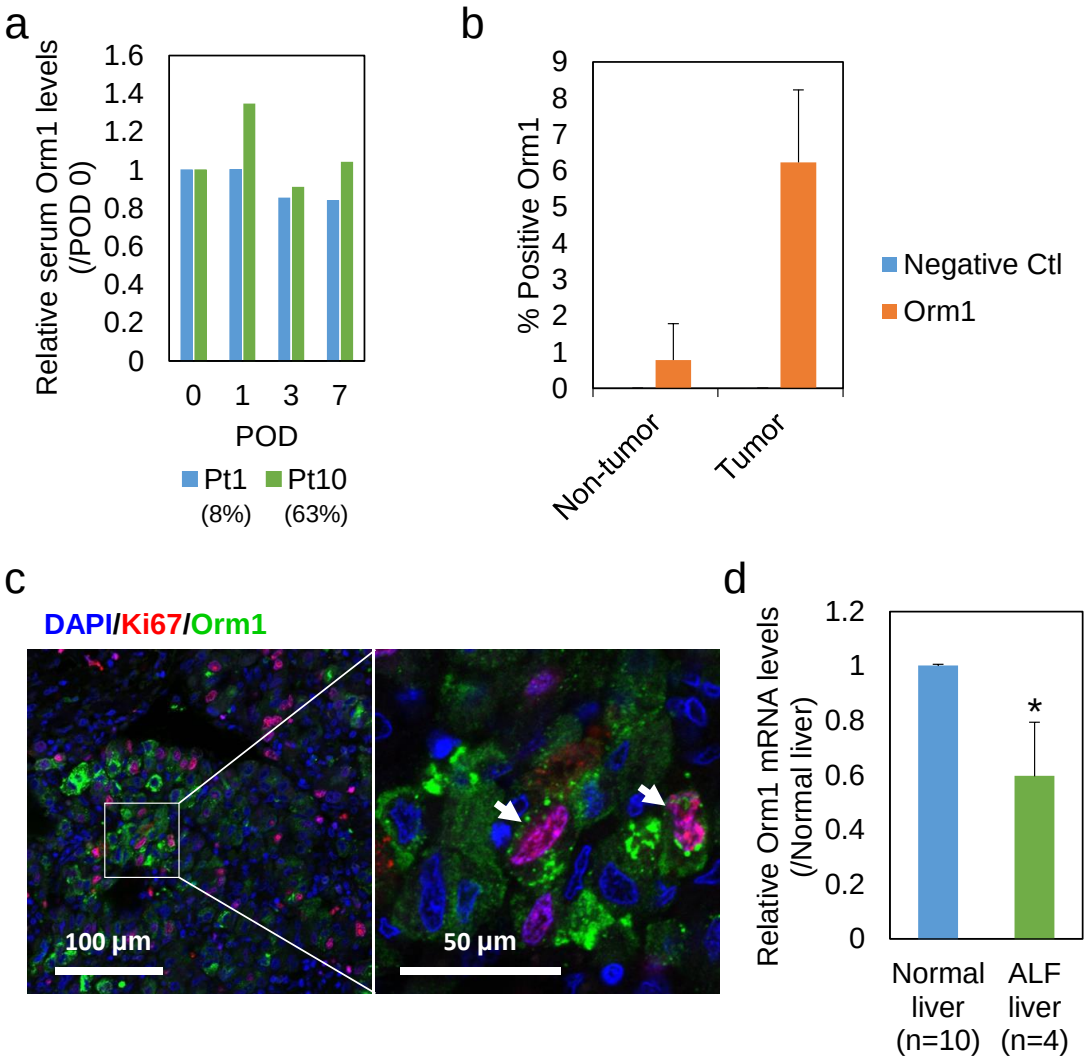

Fig. S1. Clinical expression of Orm1 in human serums and tissues. (a) Postoperative serum Orm1 changes in patients with low (Pt1, 8% resection, blue columns) and high (Pt10, 63% resection, green columns) liver resection rates. The data were presented as

fold change compared to the serum Orm1 levels at POD 0. **(b)** Quantification of the staining intensity of Orm1 in human HCC tumor and non-tumor tissues. The data were presented as average positive stained area plus the standard deviation from three different areas quantified using IHC profiler plugin in ImageJ software. The intensity values ranging from 0 to 60 were defined as positive stain. **(c)** Double immunofluorescence staining of Orm1 (green) and cell proliferation marker Ki-67 (red) in human HCC tissue. Nuclei were shown in blue (DAPI). White arrows indicate $Orm1^{+}Ki\text{-}67^{+}$ cells. **(d)** Clinical expression of Orm1 in of 10 normal livers and 4 HBV-associated ALF livers with injured liver regeneration (GSE38941).

Supplemental Figure 2

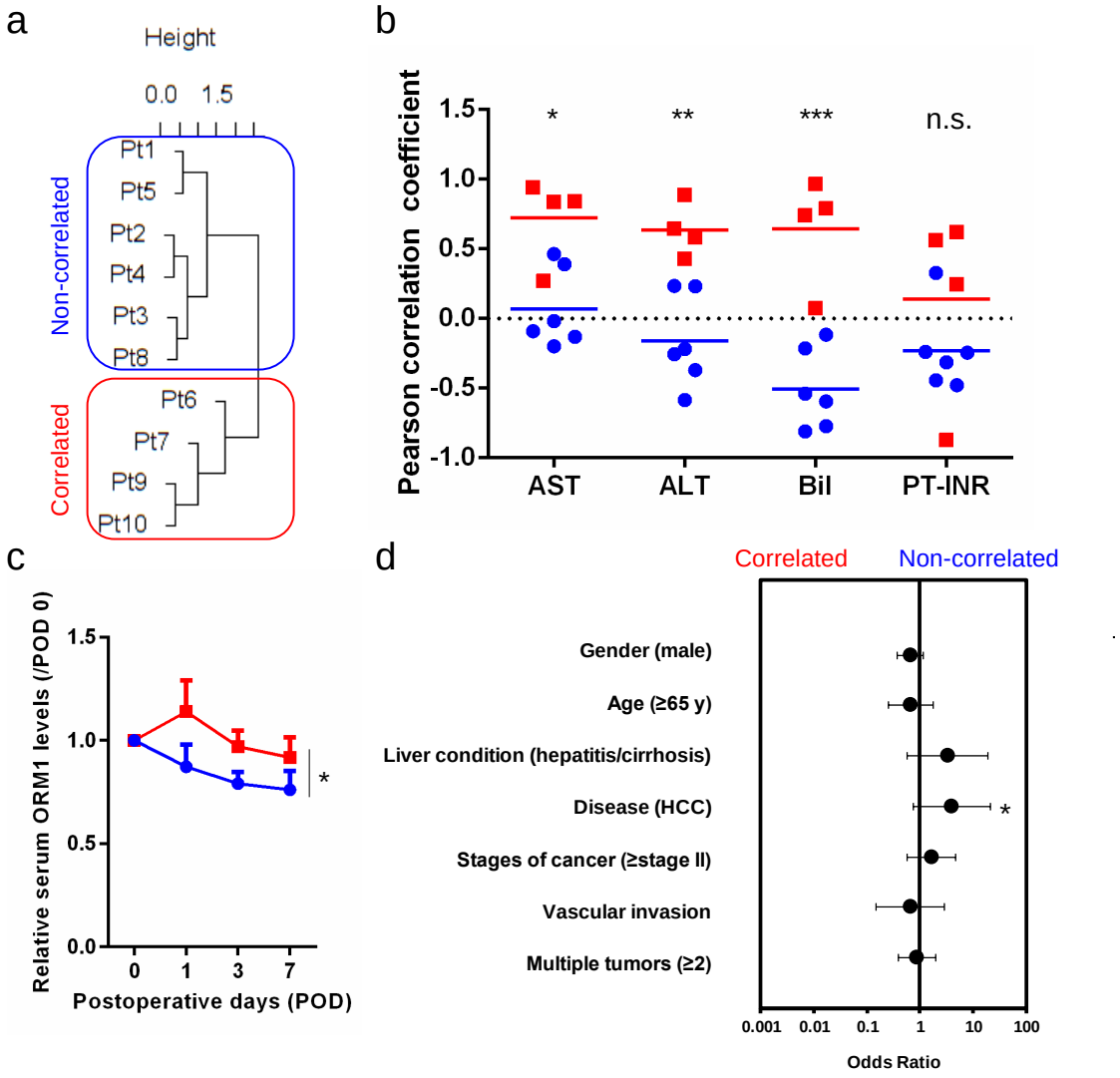

Fig. S2. Correlation of postoperative serum Orm1 levels with biomarkers of liver function. (a) Hierarchical cluster analysis discriminated the 10 patients who had undergone liver resection for HCC into two groups (the "Correlated" and "Non-correlated"

groups) using the Pearson correlation coefficients **(b)** between postoperative serum changes of Orm1 and liver function biomarkers (ALT, AST, Bil and PT.INR). **P*<0.05; ***P*<0.001; ****P*<0.0001 in two-tailed Student's *t*-test. **(c)** Comparative analysis of serum Orm1 changes post liver resection between the “Correlated” and “Non-correlated” groups. **P*<0.05 in two-way ANOVA. **(d)** Characteristics and risk factor analysis between the “Correlated” and “Non-correlated” groups. **P*<0.05 in chi-square test.

Supplemental Figure 3

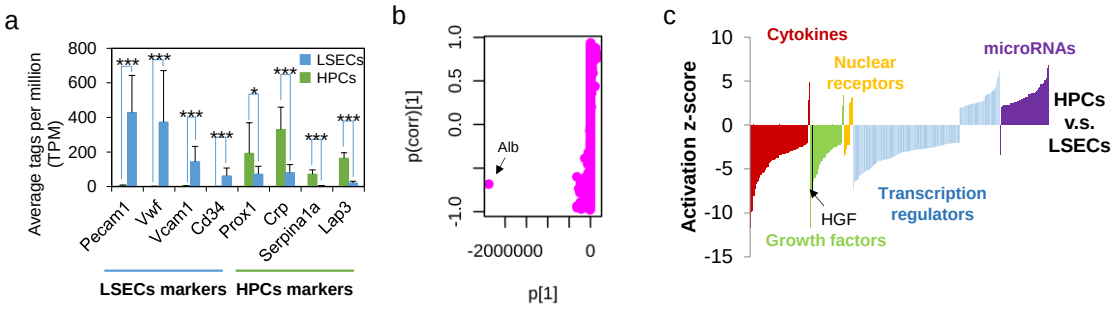

Fig. S3. Transcriptional comparison between LSECs and HPCs. (a) Expression of LSECs and HPCs markers. *P<0.05; ***P<0.0001 in two-tailed Student's t-test. The quantitative data were presented as the mean plus the standard deviation. **(b)** OPLS-DA loading S-plots were applied to the transcriptome profiles of LSECs and HPCs. S-plot illustrating the modelled covariance (p[1]) and correlation (pcorr[1]) of variables in LSECs and HPCs. The p[1] describes the magnitude of each variable, while the pcorr[1] represents the reliability of each variable. Key genes related to the discrimination between LSECs and HPCs were highlighted in the S-plot and their expression measured by CAGE analysis was presented. **(c)** Upstream regulator analysis of differentially expressed genes between LSECs and HPCs using the IPA program. An activation z-score was used as the statistical measure to predict the activation state (either activated or inhibited). An

absolute z-score more than 2 was considered as significant.

Supplemental Figure 4

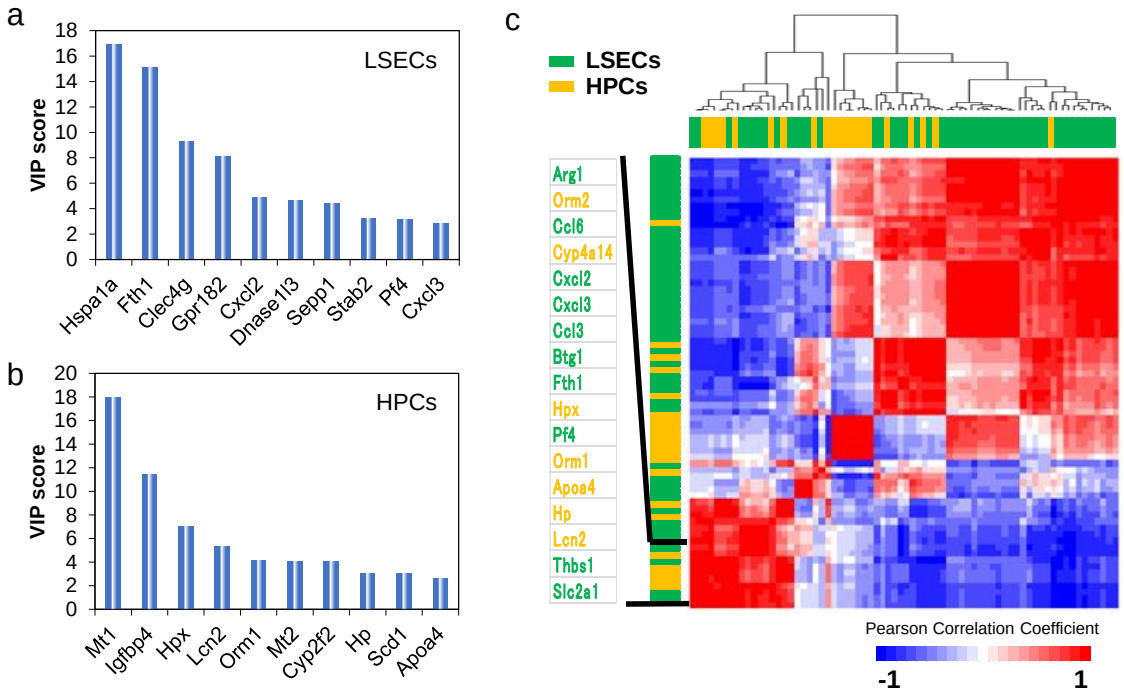

Fig. S4. Transcriptional interaction between LSECs and HPCs during liver regeneration. The genes with top VIP values of the X variables in LSECs **(a)** and HPCs **(b)** identified in PLS-DA modeling**. (c)** Pearson's correlation coefficients were calculated between the selected LSECs and HPCs genes with a VIP value more than 1.

Supplemental Figure 5

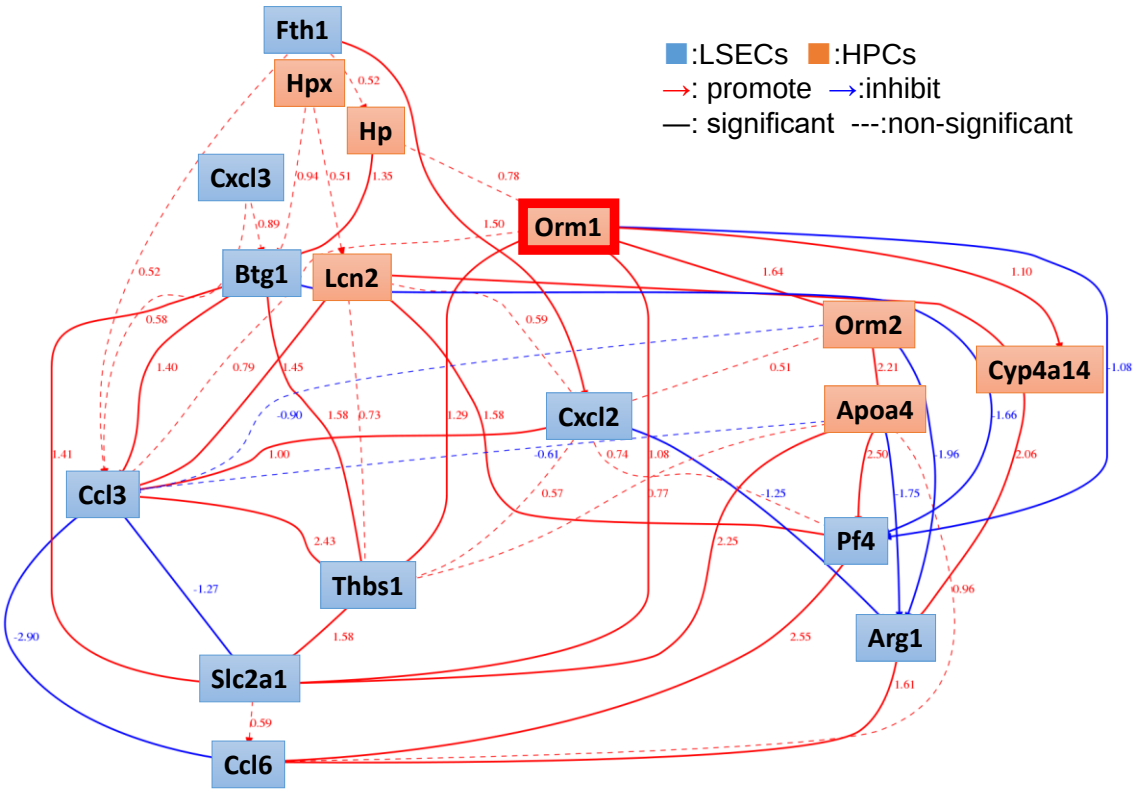

Fig. S5. Causal network model for the transcriptional interaction between LSECs and HPCs during liver regeneration. Bayesian network analysis was performed on the dataset of highly correlated LSECs and HPCs genes using the TAO-Gen algorithm. The causal relationship between each gene was evaluated in terms of a probabilistic inference. The β-value of the Bayesian model was expressed as a red arrow if positively relative and a blue arrow if negatively relative. The Orm1 in HPCs was located at the top of the

network hierarchy and significantly related directly or indirectly to most of the evaluated genes.

Supplemental Figure 6

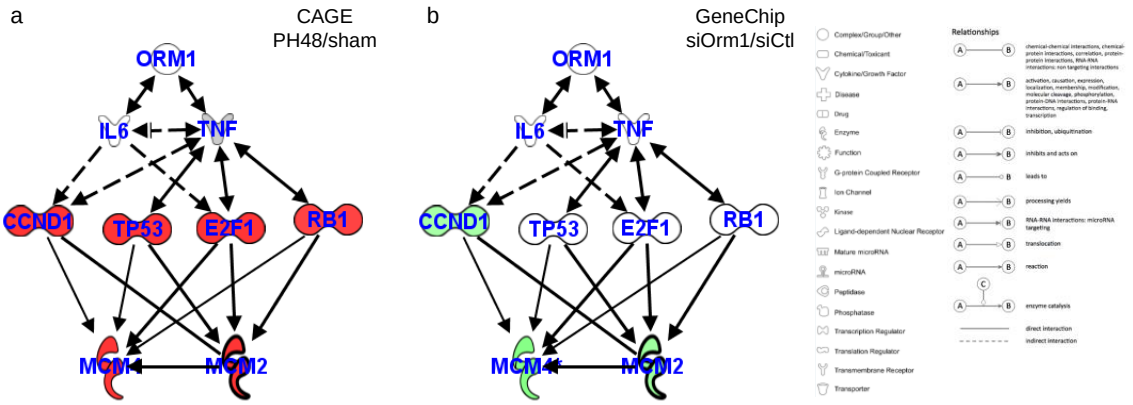

Fig. S6. Molecular basis underlying the regulatory effect of Orm1 on MCM gene expression. The tool "Path Explorer" was used to search for documented molecular interactions based on the IPA database. The tool "Overlay" was used to upload gene expression data measured using **(a)** CAGE analysis in primary HPCs isolated mouse livers at 48 h after PH and at 2 h after sham operation **(b)** microarray analysis in siCtl and siOrm1-injected mouse livers at 48 h after PH. Red, upregulated genes; green, downregulated genes.

Supplemental Figure 7

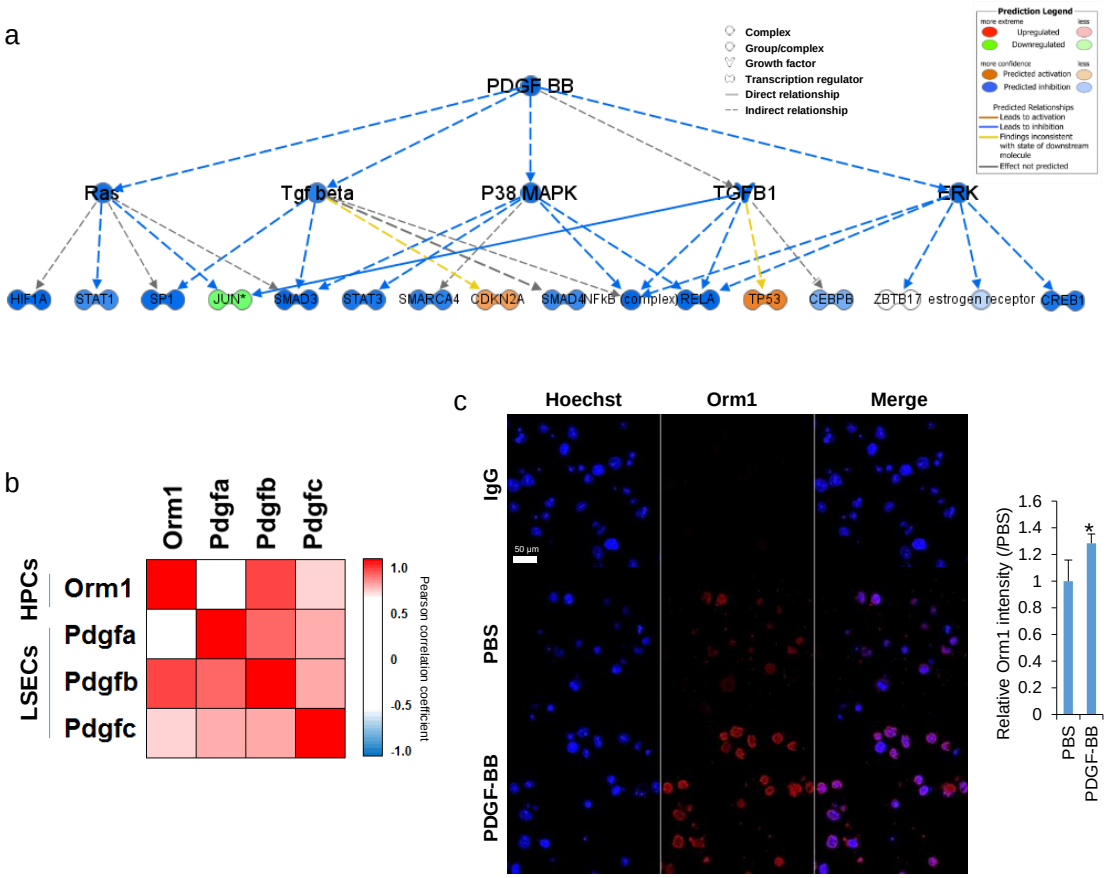

Fig. S7. Relationship between PDGFs and Orm1 in regenerating mouse livers. (a) Upstream regulator analysis performed in IPA platform based on the differentially expressed genes with a fold change of more than 2 in the livers between groups of mice receiving siOrm or siCtl. **(b)** Pearson's correlation coefficients among the gene expression of *Orm1* in HPCs and *Pdgfa*, *Pdgfb*, and *Pdgfc* in LSECs during liver regeneration

measured by CAGE analysis. **(c)** Inductive effect of PDGF-BB on Orm1 protein levels in primary mouse HPCs. Cell average Orm1 intensity was quantified in MetaXpress Image Analysis software. The *P*-value was assessed using two-tailed Student's t-test. Representative images of the immunostaining of Orm1 in primary mouse HPCs 48 h after treated with PBS and 20 ng/mL PDGF-BB. Orm1 staining was shown in red and nuclei in blue (Hoechst). Scale bar, 50 μm. The quantitative data were presented as the mean plus the standard deviation.